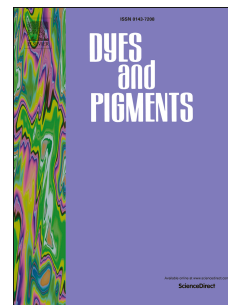


Journal Pre-proof

New Chromenylum–cyanine based dual channel chemosensors for copper and hypochlorite sensing

Kaan Karaoglu, Kerem Kaya, Ismail Yilmaz



PII: S0143-7208(20)30693-8

DOI: <https://doi.org/10.1016/j.dyepig.2020.108445>

Reference: DYPI 108445

To appear in: *Dyes and Pigments*

Received Date: 17 March 2020

Revised Date: 9 April 2020

Accepted Date: 10 April 2020

Please cite this article as: Karaoglu K, Kaya K, Yilmaz I, New Chromenylum–cyanine based dual channel chemosensors for copper and hypochlorite sensing, *Dyes and Pigments* (2020), doi: <https://doi.org/10.1016/j.dyepig.2020.108445>.

This is a PDF file of an article that has undergone enhancements after acceptance, such as the addition of a cover page and metadata, and formatting for readability, but it is not yet the definitive version of record. This version will undergo additional copyediting, typesetting and review before it is published in its final form, but we are providing this version to give early visibility of the article. Please note that, during the production process, errors may be discovered which could affect the content, and all legal disclaimers that apply to the journal pertain.

© 2020 Published by Elsevier Ltd.

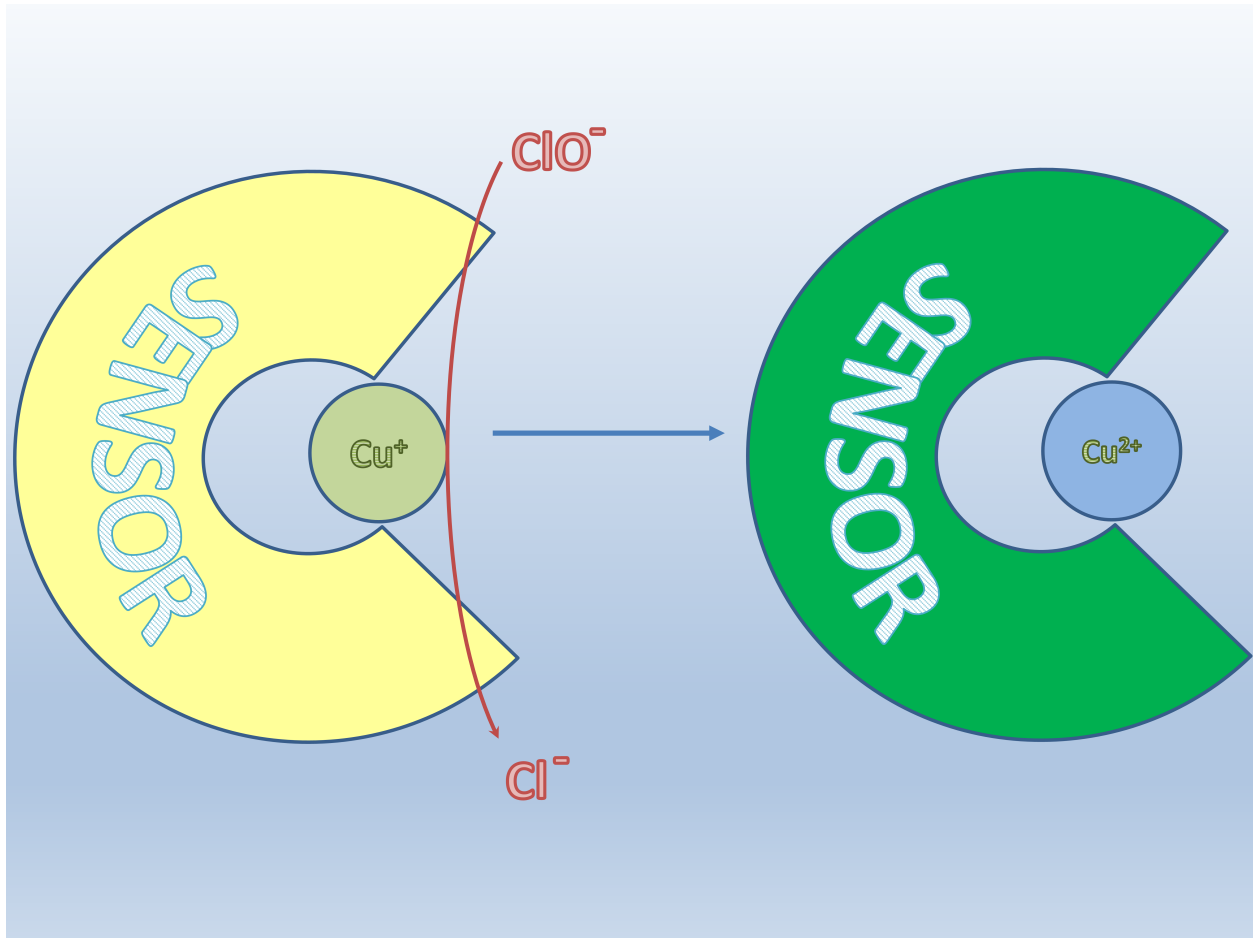
CRedit authorship contribution statement

Kaan Karaoglu: Conceptualization, Methodology, Validation, Investigation, Writing - Original Draft

Kerem KAYA: Investigation- single crystal X-ray diffraction.

Ismail Yilmaz: Conceptualization, Supervision, Writing - Review & Editing

Journal Pre-proof



New Chromenylium–cyanine Based Dual Channel Chemosensors for Copper and Hypochlorite Sensing

Kaan KARAOGLU^{1*}, Kerem KAYA², Ismail YILMAZ²

¹Recep Tayyip Erdogan University, Vocational School of Technical Sciences, Department of Chemistry and Chemical Process Technology, 53100, Rize, Turkey

²Istanbul Technical University, Department of Chemistry, 34469, Maslak, Istanbul, Turkey

Abstract

Based on a change in optical properties of chromenylium–cyanine Schiff base derivatives (**5a-c**), a series of colorimetric dual sensors have been for the first time designed, synthesized and characterized to monitor Cu²⁺ and OCl⁻ ions at near-IR (NIR) region in aqueous samples. The colorimetric responses of the sensors toward Cu²⁺ and OCl⁻ ions were evaluated for aqueous samples within a series of the competitive anions and cations at pH 7.2. The sensors detected Cu²⁺ selectively via Cu²⁺-promoted spirocyclic ring–opening reaction while photophysical change during OCl⁻ recognition is due to the spirocyclic ring–opening reaction by coordination Cu²⁺ ion generated from reaction between Cu⁺ and hypochlorite ions in analysis media. Mass and IR data suggest a 1:1 complex formation between Cu²⁺ and the receptor via phenolic O atom, N atom from Schiff base and O atom from spirocycle form. The detection limits of the dual sensors (**5a-c**) were determined to be 3.3×10⁻⁸ M, 1.93×10⁻⁸ M and 2.36×10⁻⁸ for Cu²⁺ determination and 2.83×10⁻⁸ M, 2.10×10⁻⁸ M and 2.60×10⁻⁸ M for OCl⁻ determination, indicating a high sensitivity of the sensors for Cu²⁺ and OCl⁻ detection. Additionally, we present the first single-crystal structure analysis of a chromenylium-cyanine Schiff base in this study.

Keywords: Hypochlorite sensing, Near-IR chemosensor, Chromenylium-cyanine

*Corresponding author, Tel.: +90(464)223 6126

E-mail address: kaan.karaoglu@erdogan.edu.tr (K. KARAOGLU)

Journal Pre-proof

1. Introduction

Hypochlorite (OCl^-) is one of the most used oxidizing agents in a wide range from industrial processes to household cleaning. Although the human immune system generates OCl^- from hydrogen peroxide and chloride ion by myeloperoxidase enzyme to protect the body from pathogens, the accumulation of OCl^- to the body can result in illnesses such as cardiovascular diseases, inflammatory reactions, arthritis, and cancer. Thus, the development of sensitive and selective sensors for OCl^- sensing in water samples is of great importance [1–3]. One of the sophisticated methods for OCl^- detection includes the use of rhodamine-based (Cu^{2+}) sensors which generate an optical response based on the spirocyclic ring-opening reaction [4–6]. In this method, Cu^{2+} is generated by oxidation of Cu^+ ions upon the addition of OCl^- , then an absorption band is observed corresponding to Cu^{2+} -promoted spirocyclic ring-opening reaction [7,8]. To this end, various rhodamine B-based sensors have been developed in recent years, and these derivatives exhibit a characteristic intense absorption band with a maximum at about 550 nm [9–12]. In order to decrease photodamage in vivo, chromenylum-cyanine based chemosensors have been designed for metal ion sensing [13–17].

However, to the best of our knowledge, chromenylum-cyanine based OCl^- sensing has been never reported. In this study, we design and synthesize some chromenylum-cyanine chemosensors to detect selectively OCl^- ion in aqueous samples, via Cu^{2+} promoted the ring-opening reaction. In order to achieve this goal, first, we investigated the selectivity of the sensors to Cu^{2+} ion, and then performed a series of experiments in order to evaluate OCl^- sensing properties of the sensors. The spectrometric assays showed that the sensor is highly sensitive and selective to OCl^- in the near-IR region. The chemical structures of chemosensors have been characterized by FT-IR, UV-Vis, ^1H - and ^{13}C -NMR, mass spectrometry. We also present the first single-crystal structure analysis of a chromenylum-cyanine Schiff base.

2. Experimental

2.1. Materials and apparatus

The solutions of Na^+ , K^+ , Mg^{2+} , Ca^{2+} , Mn^{2+} , Fe^{3+} , Co^{2+} , Ni^{2+} , Cu^{2+} , Zn^{2+} , Al^{3+} , Cd^{2+} , Hg^{2+} and Pb^{2+} ions in water were prepared freshly for each measurement from their nitrate salts except for Mn^{2+} was prepared acetate salt. Aqueous solutions of sodium salts of F^- , Cl^- , Br^- , I^- , CH_3COO^- , CO_3^{2-} , ClO^- , NO_2^- , NO_3^- , PO_4^{3-} , HSO_3^- and SO_4^{2-} at 1×10^{-3} M were prepared in deionized water and stored in amber glass bottles. 3-Diethylaminohanol, phthalic anhydride, hydrazine hydrate, 2,4-dihydroxybenzaldehyde and (benzotriazol-1-yl)tris(dimethylamino)phosphonium hexafluorophosphate were obtained from Sigma Aldrich.

Fourier transform infrared (FT-IR) spectra were recorded on a Perkin Elmer Spectrum 100 spectrometer equipped with an ATR apparatus. Mass spectra were recorded using Thermo Sci. TSQ Quantum Access MAX Triple Stage Quadrupole mass spectrometer equipped with heated electrospray ionization (H-ESI) probe at the Central Research Laboratory of Recep Tayyip Erdogan University. ^1H and ^{13}C NMR spectra were recorded on an Agilent Technologies 400/54 spectrometer at the Istanbul Technical University. UV-Vis spectra were recorded on a Perkin Elmer Lambda 35 UV-Vis spectrophotometer. HPLC analysis were carried out on a Thermo Scientific Finnigan Surveyor HPLC system equipped with photodiode array (PDA) detector. The injection volume was 20 μL and the flow rate maintained at 1.2 mL min^{-1} . A C18 column was applied for the chromatographic separation at 25 $^\circ\text{C}$ and the elution solvents were A and B containing acetonitrile-water (70:30, v/v) and acetic acid-water (2:98, v/v), respectively.

2.2. Synthesis of chemosensor (5a, 5b, and 5c)

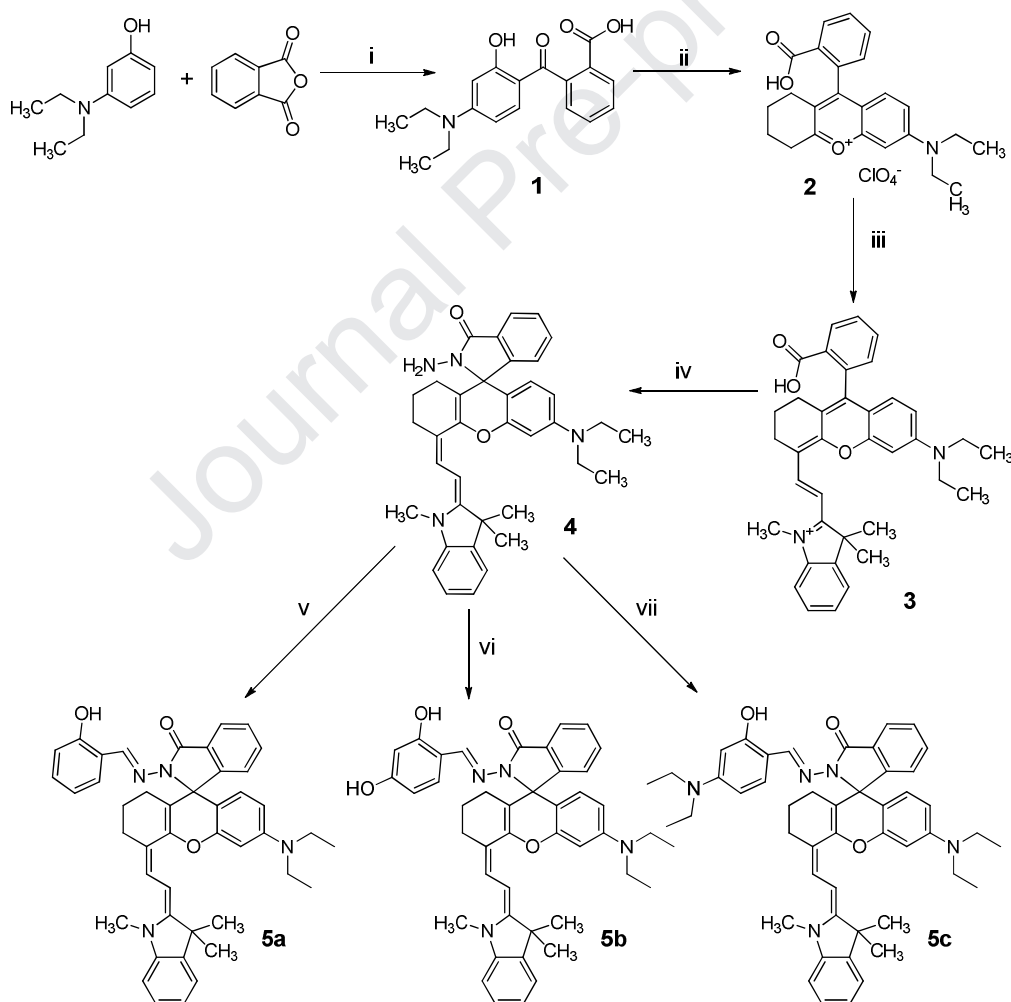
The starting hydrazide, (4'Z)-2-amino-6'-(diethylamino)-4'-{2-[(2Z)-1,3,3-trimethyl-2,3-dihydro-1H-indol-2-ylidene]ethylidene}-1',2,2',3,3',4'-hexahydrospyro[isindol-1,9'-

xanthene]-3-on, was synthesized by literature procedures [18,19]. The hydrazide (0.573 g, 1 mmol) was dissolved in absolute ethanol (10 mL) and solution purged by argon for 30 min. Then aldehyde (1.1 mmol) was added into the solution, and the mixture was stirred at room temperature for appropriate time controlled by thin-layer chromatography (TLC) (Scheme 1). The solvent was evaporated by rotary evaporator under reduced pressure to dryness, and crude product was purified by column chromatography on silica gel (EtOH/CH₂Cl₂, 1:20). Finally, an aliquot of the isolated fraction was then used to verify the purity by HPLC (Figure S. 1).

5a: Yield: 73%. Melting point: 244 °C. Color: Yellow. Rf: 0.57, EtOH/CH₂Cl₂, (1:20, v/v). Analytical data for C₄₄H₄₄N₄O₃, ESI-MS (m/z) 676.85 [M+H]⁺ (676.85 calc.). HPLC purity 98.4% (t_R=30.06 min). FT-IR (ATR, cm⁻¹): 3079, 2969, 2929, 1702, 1619, 1589, 1310, and 1124. ¹H NMR (δ, ppm): 11.13, 9.14, 7.95, 7.57–7.53, 7.49, 7.25, 7.23–7.19, 7.17, 6.90, 6.86, 6.82, 6.63, 6.46, 6.29, 6.46, 5.39, 3.35, 3.160, 2.67, 2.46, 1.76, 1.79, 1.63, 1.26, 1.18. ¹³C NMR (δ, ppm): 164.7, 158.8, 157.8, 152.5, 149.8, 148.9, 148.3, 145.4, 138.9, 133.3, 131.4, 131.3, 129.8, 128.5, 127.7, 121.5, 120.2, 119.3, 118.6, 117.1, 108.5, 105.7, 104.8, 103.3, 97.9, 92.2, 68.2, 45.5, 44.3, 29.1, 28.4, 25.3, 22.2, 12.6.

5b: Yield: 26%. Melting point: 195 °C. Color: Yellow. Rf: 0.36, EtOH/CH₂Cl₂, (1:20, v/v). Analytical data for C₄₄H₄₄N₄O₄, ESI-MS (m/z) 693.25 [M+H]⁺ (692.84 calc.). HPLC purity 96.8% (t_R= 30.14 min). FT-IR (ATR, cm⁻¹): 3056, 2969, 2929, 1687, 1622, 1589, 1313, and 1115. ¹H NMR (δ, ppm): 11.34, 9.69, 9.05, 7.93, 7.46–7.55, 7.25, 7.18, 7.01, 6.86, 6.62, 6.46, 6.39–6.33, 6.28, 5.39, 3.35, 3.16, 2.61, 2.46, 1.79, 1.76, 1.63, 1.26, 1.18. ¹³C NMR (δ, ppm): 194.2, 164.6, 160.8, 159.1, 157.7, 153.5, 152.5, 149.8, 148.9, 148.1, 145.3, 138.9, 135.1, 129.9, 128.5, 127.7, 123.8, 123.5, 121.5, 120.2, 120.0, 119.3, 112.2, 108.5, 107.5, 105.7, 104.9, 103.5, 98.0, 92.1, 68.3, 45.5, 44.3, 31.2, 28.3, 25.3, 22.1, 12.6.

5c: Yield: 36%. Melting point: 155 °C. Color: Yellow. Rf: 0.41, EtOH/CH₂Cl₂, (1:20, v/v). Analytical data for C₄₈H₅₃N₅O₄, ESI-MS (m/z) 748.25 [M+H]⁺ (747.97calc.). HPLC purity 97.9% (t_R=33.11 min). FT-IR (ATR, cm⁻¹): 3066, 2968, 2928, 1694, 1624, 1593, 1314, and 1126. ¹H NMR (δ, ppm): 11.24, 9.08, 7.91, 7.51-7.47, 7.19-7.18, 6.99, 6.85, 6.62, 6.37, 6.27, 6.16, 6.13, 5.39, 3.33, 3.15, 2.56, 2.48, 1.86, 1.83, 1.77, 1.75, 1.18, 1.14. ¹³C NMR (δ, ppm): 164.2, 160.8, 157.4, 154.8, 152.5, 150.5, 149.7, 148.7, 148.0, 145.4, 139.0, 132.9, 132.7, 130.5, 128.3, 127.7, 127.6, 123.4, 123.0, 121.5, 120.6, 119.4, 119.1, 108.4, 107.4, 105.6, 105.2, 104.0, 103.3, 98.2, 98.0, 92.3, 68.1, 45.4, 44.5, 29.1, 28.4, 25.3, 22.9, 22.2, 12.6.



Scheme 1. Synthesis scheme of the sensor. i: Toluene, 3h, 35% NaOH, 10,0 M HCl; ii: H₂SO₄, cyclohexanone, 2h; iii: 2-(1,3,3-trimethylindolin-2-ylidene)acetaldehyde; iv: hydrazine hydrate, BOP reagent; v: 2-hydroxybenzaldehyde, vi: 2,4-dihydroxybenzaldehyde, vii: 4-diethylamino-2-hydroxybenzaldehyde.

2.3. Sensing Experiments

Nitrate salts of the Na^+ , K^+ , Mg^{2+} , Ca^{2+} , Mn^{2+} , Fe^{3+} , Co^{2+} , Ni^{2+} , Cu^{2+} , Zn^{2+} , Al^{3+} , Cd^{2+} , Hg^{2+} and Pb^{2+} were used to evaluate cation sensing properties of the sensors. Stock solutions (3×10^{-3} M) of the sodium salts of F^- , Cl^- , Br^- , I^- , CH_3COO^- , CO_3^{2-} , ClO^- , NO_2^- , NO_3^- , PO_4^{3-} , HSO_3^- and SO_4^{2-} were prepared in deionized water, and 3×10^{-3} M solutions of the sensors were prepared in acetonitrile (MeCN). All the solutions were stored in amber bottles at room temperature. All the spectroscopic measurements were performed in triplicate and data are presented as the mean, with error bars reflecting the standard deviation.

Detection limit based on the standard deviation of the response and the slope by IUPAC was determined from the Eq. (1).

$$LOD = \frac{3.3 \times S_d}{S} \quad (1)$$

where S_d is the standard deviation of the blank measurements ($n=10$) and S is the slope of the calibration curve.

2.4. Single Crystal X-Ray Crystallography

The single crystal of **5a** with dimensions 0.03x0.10x0.20mm was grown by slow evaporation of ethanol solution. The crystal was mounted on a micromount and attached to a goniometer head on a Bruker D8 VENTURE diffractometer equipped with PHOTON100 detector and measured with graphite monochromated Mo-K α radiation ($\lambda = 0.71073 \text{ \AA}$) using 1.0° of Ω and ϕ rotation frames at room temperature (295K). The structure has been solved by intrinsic method SHELXS-1997 [20] and refined by SHELXL-2014/7 [21]. Molecular drawings are generated using OLEX2. Ver. 1.2-dev [22].

3. Results and Discussion

In order to evaluate effect of electron-donating/withdrawing group for complexation, Schiff bases of chromenylium-cyanine (**5a-5c**) from 2-hydroxybenzaldehyde, 2,4-hydroxybenzaldehyde and 4-diethylamino-2-hydroxybenzaldehyde were synthesized. Spectral data obtained for the sensors were in accordance with our previous study [17]. Characteristic C=O stretching modes of spirocycle were observed at about 1690 cm^{-1} for the sensors in FTIR spectra. Bands at about 1620 cm^{-1} were also assigned to C=N stretching of imine bond. The disappearance of the carbonyl band and the shift of the imino stretching to $\sim 1600\text{ cm}^{-1}$ clearly suggest complexation of the Cu^{2+} (Figure S. 2–Figure S. 5) [23]. The chemical structures of the sensors were also confirmed by NMR spectra. In the ^1H NMR spectra of the **5a**, –OH proton and imine proton signals were observed as a singlet at 11.132 and 9.140 ppm, respectively. Proton signals of H46 and H34 were observed at 5.391 and 6.459 ppm, for atom labels see structure in Figure S. 6. The signals of methyl protons of H1, H39, H37 and H38 were observed as singlets at 1.1180, 3.160, 1.759, and 1.788 ppm, respectively. A doublet of quartet ($J=5.6\text{ Hz}$, $J=1.6\text{ Hz}$) appeared at 3.351 ppm which assigned to H2 and H5 protons. The signals of aromatic protons were in the range of 6.339–7.952 ppm. ^1H NMR signals of the H16, H17 and H17 were observed at 2.607–2.456, 1.256 and 1.627 ppm, respectively [24]. The ^1H NMR spectra of **5b** and **5c** are similar that of **5a** and differ only in substituted group at the para-position of the imine moiety (Figure S. 6–Figure S. 9). The characteristic ^{13}C NMR signals of carbonyl (C32) and the C12 corresponding to spirocycle closed form of **5a** were observed at 164.378 and 68 ppm, respectively (Figure S. 6–Figure S. 9). The similar spectral features were observed for **5b** and **5c**. The mass peaks of positive ions were detected at m/z 677.16, 693.25 and 748.25, corresponding to the protonated molecular ions for **5a**, **5b** and **5c**, respectively (Figure S. 10–Figure S. 12). Molecular structure of the **5a-Cu²⁺** complex has been also investigated by ESI mass spectra (Figure S. 13). The molecular ion peak for the

complex structure was observed at 769.77 m/z, which confirmed the formation of a 1:1 complex of **5a** with Cu²⁺. Mass data were consistent with IR data that suggest coordination between Cu²⁺ and phenolic O atom, N atom from Schiff base and O atom from spirocycle (Figure S. 14).

Compound **5a** was structurally characterized by single crystal X-ray diffraction, and thermal ellipsoids are plotted in Figure 1. Figure 2 shows the crystal packing of the structure showing π — π interaction and Figure 3 shows the intra- and intermolecular hydrogen bonding of the crystal lattice.

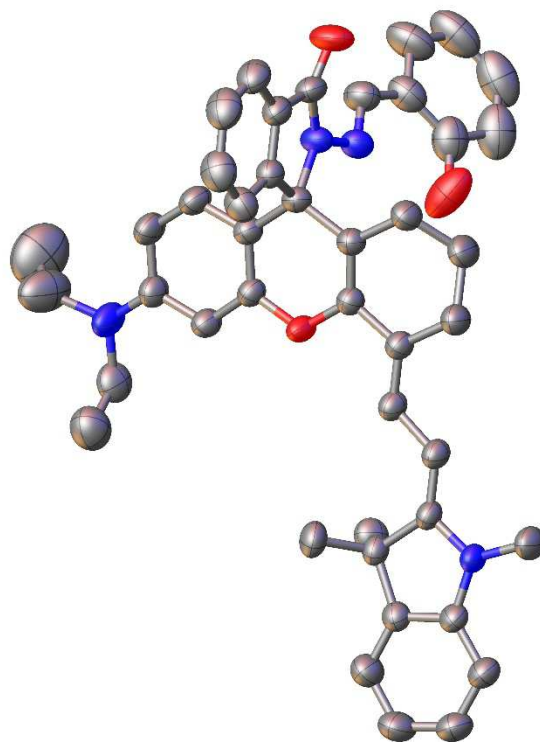


Figure 1. Thermal ellipsoids of **5a** are drawn at 50% probability. Hydrogen atoms are omitted for clarity.

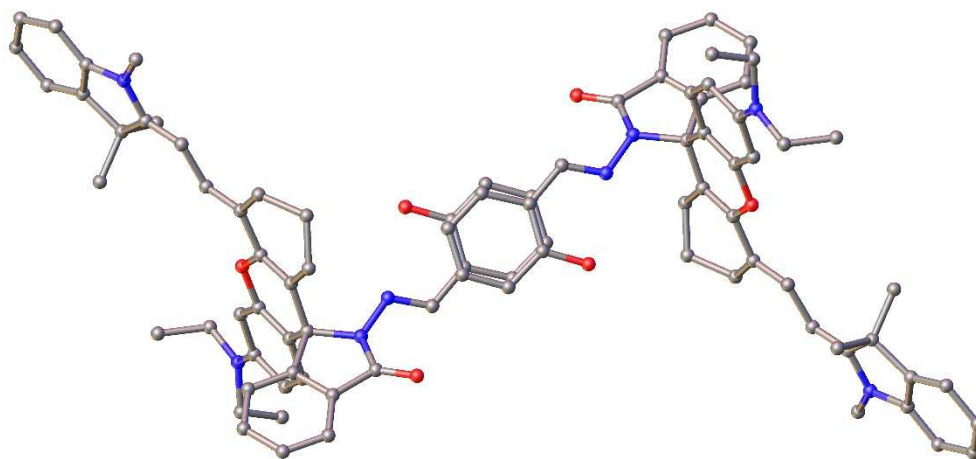


Figure 2. Face-to-face π - π stacking occurring between phenoxy units of structure **5a**.

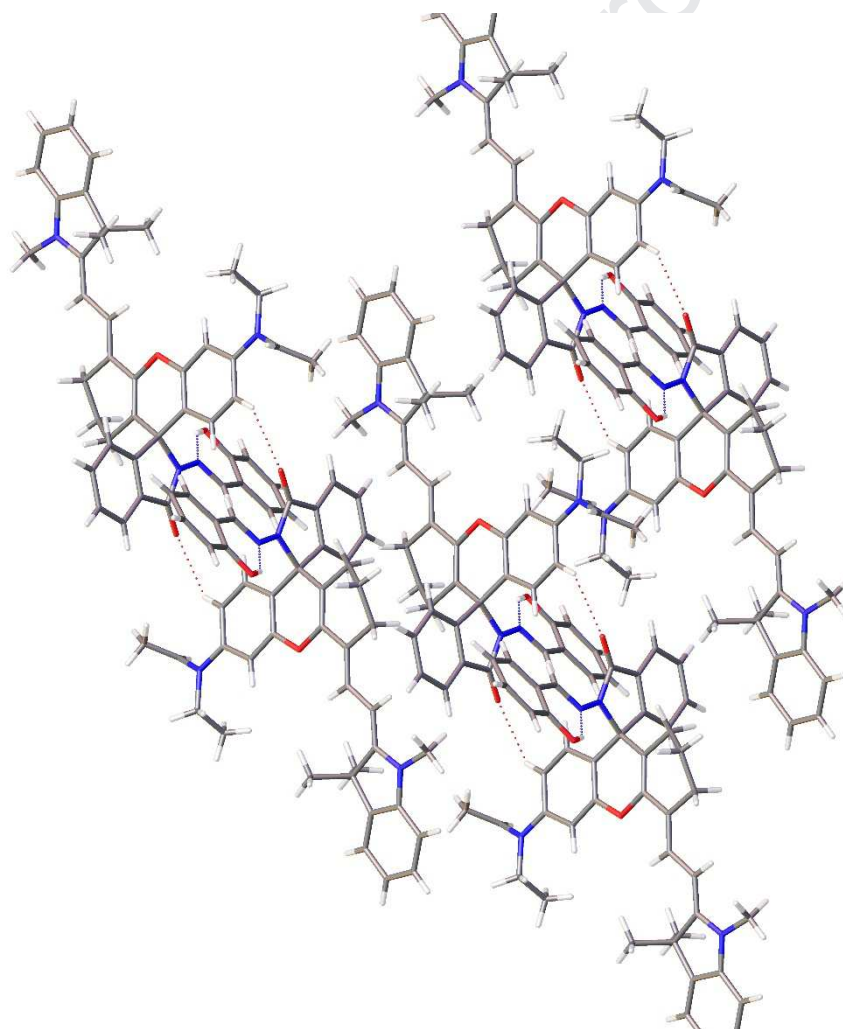


Figure 3. Intra- and intermolecular hydrogen bonding of the crystal structure **5a**.

The crystal data and structure refinement parameters of **5a** are given in Table 1. Table S. 1 contains the selected bond lengths, bond and torsion angles for **5a**. Table S. 2 contains the hydrogen bonding geometries. CCDC 1985102 contains the supplementary crystallographic data for **5a**. Further details on crystal data, data collection, and refinements can be found in the supporting information.

Journal Pre-proof

Table 1. Crystal data and structure refinement parameters for **5a**.

	5a
Empirical formula	C ₄₄ H ₄₄ N ₄ O ₃
Formula weight (g/mol)	676.83
T(K)	295(0)
λ(Å)	0.71073
Crystal system	Triclinic
Space group	P - 1
Unit cell dimensions: (Å, °)	
a	11.8062(15)
b	12.3990(16)
c	12.8593(16)
V(Å³)	1838.3(4)
α	92.222(3)
β	102.121(3)
γ	91.095(3)
Z	2
Absorption coefficient (mm⁻¹)	0.077
Dcalc (g/cm³)	1.223
F(000)	720
Crystal size (mm)	0.03 x 0.10 x 0.20
θ range for data collection (°)	2.13 to 25.00
Index ranges	-13 ≤ h ≤ 14 -14 ≤ k ≤ 14 -15 ≤ l ≤ 15
Reflections collected	48124
Independent reflections	6471
Coverage of independent reflections (%)	99.9
Data/parameters	6471/ 465
Max. and min. transmission	0.998 - 0.991
Final R indices [$I \geq 2\sigma(I)$]	R1 = 0.0685 wR2 = 0.1243
R indices (all data)	R1 = 0.1576 wR2 = 0.1584
Goodness-of-fit on F²	1.009

R1: agreement between the calculated and observed models, wR2: squared F-values.

5a crystallized in a triclinic crystal system with P-1 space group. Each unit cell contains two molecules (Z=2). The crystal lattice is strongly stabilized by intra- and intermolecular hydrogen bonding, also by π — π stacking which can be seen in Figure 2 and Figure 3,

respectively. Xanthene moiety and isoindole unit having imine functionality are nearly perpendicular to each other with a dihedral angle of 86.54° . On the other hand, xanthene and isoindole having quaternized ammonium are nearly coplanar with a dihedral angle of 2.03° . C34-C45 single bond of $1.44(6)$ Å is much shorter than average carbon-carbon single bond of 1.54 Å which shows the extended π -conjugation of the system. Carbon atoms of the diethylamine groups contain minor disorders. The intramolecular hydrogen bonding occurs between phenoxy hydrogen and imine nitrogen. The intermolecular hydrogen bonding occurs between phenyl hydrogen and carbonyl oxygen of a neighbour molecule. A strong face-to-face π – π interaction occurs between neighbour phenyl units with 3.92 Å centroid-to-centroid distance and a shift of 0.93 Å. C39-N4 distance of $1.44(4)$ Å belonging to the ammonium unit is shorter than similar crystals found in the literature.⁵⁻⁷ This also proves the extended π -system of the molecule. N1-N2 distance of $1.38(4)$ Å and C25-O2 double bond distance of $1.22(5)$ Å belonging to the carbonyl unit shows that the keto tautomer is dominant in the structure.

3.1. Response of the chemosensors to cations and anions

Sensing properties of the sensors were tested within a series of mono-, di- and trivalent metal ions in MeCN/HEPEs buffer (2:1, v/v, pH 7.2). In order to determine selectivity of the sensors at room temperature, 1×10^{-5} M solution of the sensor was used each time in the presence of 5 equivalents of different metal ions. The UV–Vis. spectra of the sensors show a very weak absorption band between 625 and 750 nm, and an absorption band located at 711 nm was significantly enhanced upon addition of Cu^{2+} ion (Figure 4A) [25,26]. Other metal ions, Na^+ , K^+ , Mg^{2+} , Ca^{2+} , Cr^{2+} , Mn^{2+} , Fe^{3+} , Co^{2+} , Ni^{2+} , Cu^{2+} , Zn^{2+} , Al^{3+} , Cd^{2+} , Hg^{2+} and Pb^{2+} , did not cause any significant changes under the identical conditions. The sensors detected Cu^{2+} selectively via Cu^{2+} -promoted spirocyclic ring–opening reaction.

To investigate the selectivity of the sensor in the presence of competitive metal ions, such as Na^+ , K^+ , Mg^{2+} , Ca^{2+} , Cr^{2+} , Mn^{2+} , Fe^{3+} , Co^{2+} , Ni^{2+} , Cu^{2+} , Zn^{2+} , Al^{3+} , Cd^{2+} , Hg^{2+} and Pb^{2+} , the experiments were performed by addition of 1.0 equiv. of Cu^{2+} to solutions containing 5.0 equivalent of other metal ions in MeCN/HEPEs buffer (2:1, v/v, pH 7.2) media. The selectivity experiments for mono-, di-, and trivalent cations showed that none of the competitive metal ions had no obvious interference with the detection of Cu^{2+} , and indicated the good selectivity of the sensor for Cu^{2+} ion (Figure 4B). Details of the sensing properties of **5a** and **5c** were given in Supplementary materials (Figure S. 21–Figure S. 22)

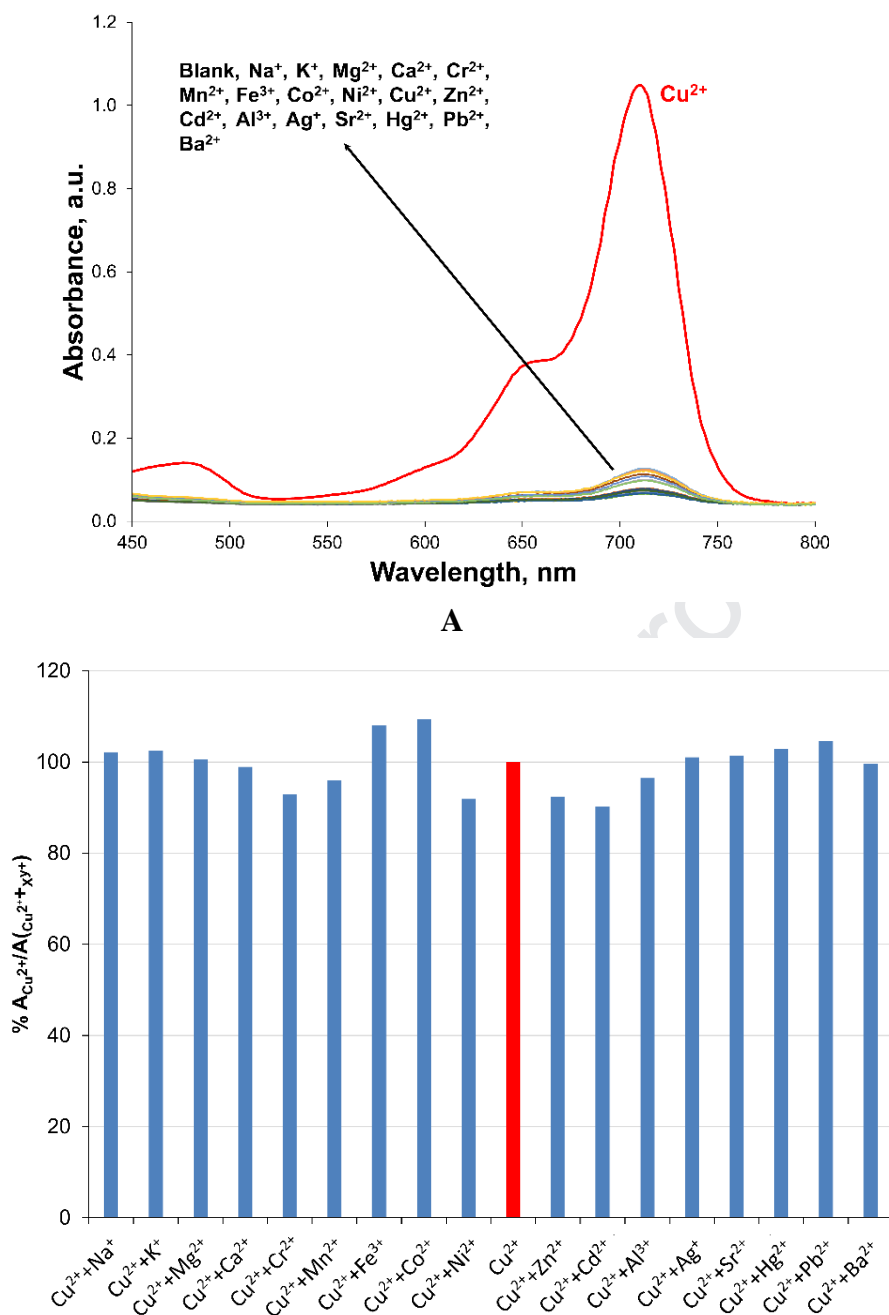


Figure 4. UV-vis. experiments of **5b** (1.0×10^{-5} M) in MeCN/H₂O (2:1, v/v, pH 7.2); **A**) absorption spectra of the sensor in the presence of 5×10^{-5} M metal ions **B**) Absorbance of the sensor (1.0×10^{-5} M) with Cu²⁺, followed by 5 equivalent of competitive metal ions.

The instant response of the sensor to Cu²⁺ enables determination of the detection limit of the sensor by titration experiments. The titration experiments were performed by

successive additions of 2 μL solution of Cu^{2+} ion to 1×10^{-5} M sensor solution at pH 7.2 in HEPES buffer media (Figure 5)

The detection limits of the **5a**, **5b** and **5c** were determined to be 3.3×10^{-8} M, 1.93×10^{-8} M and 2.36×10^{-8} M, respectively, indicating a high sensitivity of the sensors for Cu^{2+} . For comparison, literature data are given in Table 2. These results indicated that the sensors **5a-c** can serve as a potential candidate of a “naked-eye” chemosensor for Cu^{2+} in aqueous media.

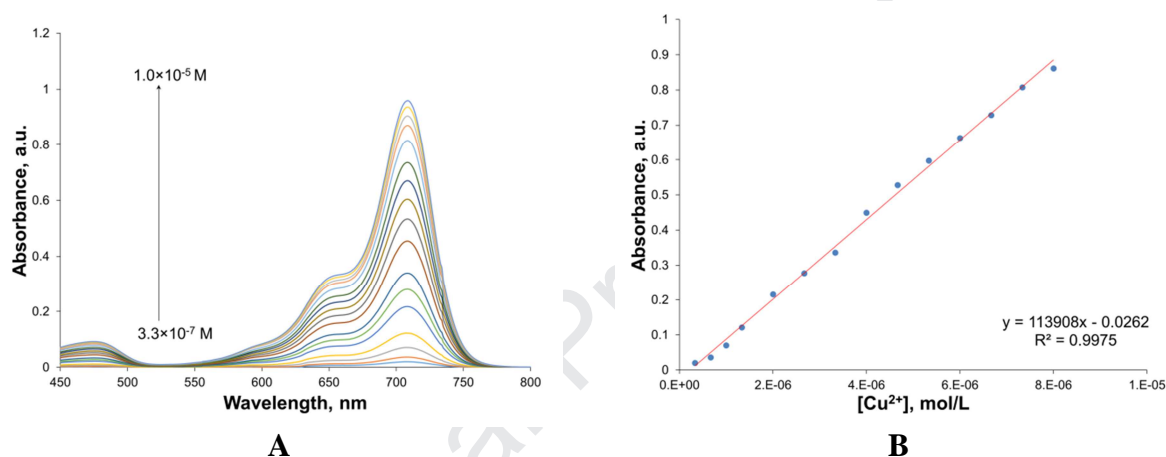


Figure 5. UV–vis titration experiments of **5b** (1.0×10^{-5} M) in MeCN/ H_2O (2:1, v/v, pH 7.2) **A**) with Cu^{2+} **B**) the titration curve derived from the titration with Cu^{2+} at 711 nm.

Table 2. A comparison table about the detection limits for Cu^{2+} .

Structure	Working range, mol L ⁻¹	LOD, mol L ⁻¹	Reference
Rhodamine B	1.0×10^{-5} to 3.0×10^{-4}	3.42×10^{-6}	[27]
Rhodamine B	NA	1.63×10^{-6}	[28]
Chromenylum-cyanine	0 to 5.0×10^{-6}	5.00×10^{-8}	[29]
Chromenylum-cyanine	3.3×10^{-7} to 1.0×10^{-5}	2.36×10^{-8}	This work
Chromenylum-cyanine	1.0×10^{-7} to 6.0×10^{-7}	1.50×10^{-8}	[30]

NA: Not available

It was found that the sensors formed colorless solutions with cuprous ions in 1:2(v/v) water/ MeCN at pH = 7.2. Upon addition of hypochlorite to these solutions, an absorption peak centered at 711 nm appeared as a result of the formation of Cu^{2+} by *in situ* oxidation of

Cu^+ ion (Figure 6). In order to evaluate the hypochlorite sensing properties of the sensors via $\text{Cu}^+ \rightarrow \text{Cu}^{2+}$ oxidation, the same experimental procedure adopted for metal sensing properties were performed using common anions (F^- , Cl^- , Br^- , I^- , CH_3COO^- , ClO^- , CO_3^{2-} , NO_2^- , NO_3^- , PO_4^{3-} , HSO_3^- and SO_4^{2-}) and H_2O_2 , one of the reactive oxygen species, in water (Figure 7).

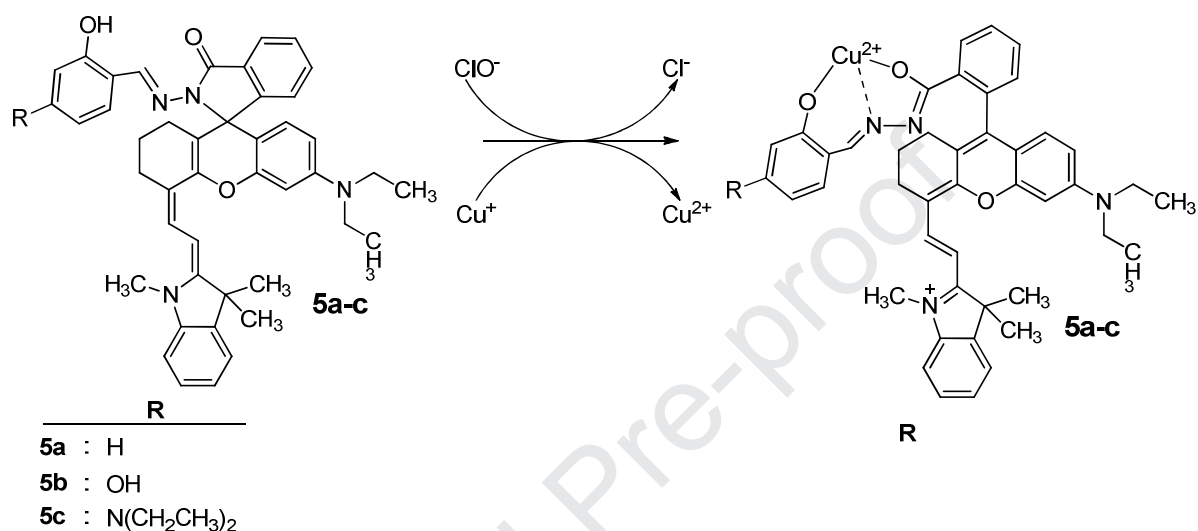


Figure 6. Proposed spirocyclic ring-opening reaction induced by $\text{Cu}^+/\text{Cu}^{2+}$ oxidation.

Absorption behaviors of blank samples were investigated in both some common solvents (Figure S. 18) and different temperatures (Figure S. 19). It was found by spectrophotometric analysis that stability of the cuprous ions was higher in MeCN. Temperature dependencies of the sensors were also investigated in the same media, and significant absorption changes for blank samples were observed by increasing temperature. Thus, all the spectrophotometric experiments were performed at 25 °C in MeCN/water mixture. Sodium ascorbate was used to stabilize cuprous ions in analysis media, and ascorbate: Cu^+ ratio was optimized as shown in Figure S. 20. The optimum concentrations of Cu^+ and sodium ascorbate were determined as 1.0×10^{-4} M and 4.0×10^{-6} M, respectively. The optical responses of the sensors toward ClO^- were analyzed in MeCN/ H_2O (2:1, v/v, pH 7.2) at pH 7.2 applying 5 minutes incubation time. In order to determine selectivity of the sensors

at room temperature, 1×10^{-5} M solution of the sensors was used each time in the presence of 5 equivalents of F^- , Cl^- , Br^- , I^- , CH_3COO^- , ClO^- , H_2O_2 , CO_3^{2-} , NO_2^- , NO_3^- , PO_4^{3-} , HSO_3^- and SO_4^{2-} . The colorimetric responses of the **5a**, **5b** and **5c** to OCl^- ion were given in Figure 7. The more intense absorption bands were obtained for OCl^- ion for all the sensors while the other anions, showed negligible absorption bands. However, selectivity experiments indicated that the presence of 5-fold excess of H_2O_2 caused interference by oxidation of Cu^+ ion to Cu^{2+} . The sensors responded to H_2O_2 , although not as well as in the case of ClO^- . Because of weaker oxidation capacity of the H_2O_2 than ClO^- , the observed absorbance change is much lower than that in the presence of ClO^- [7].

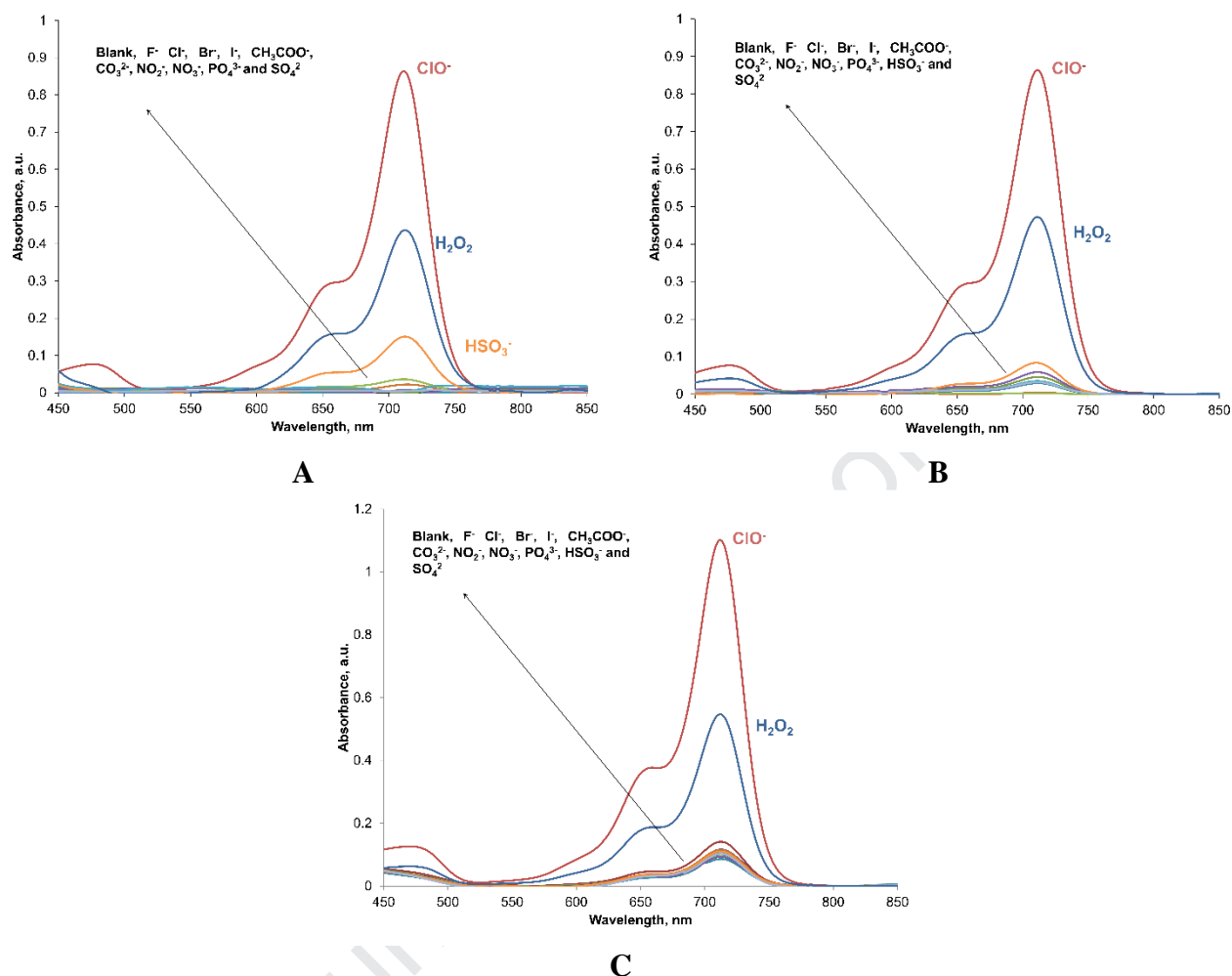
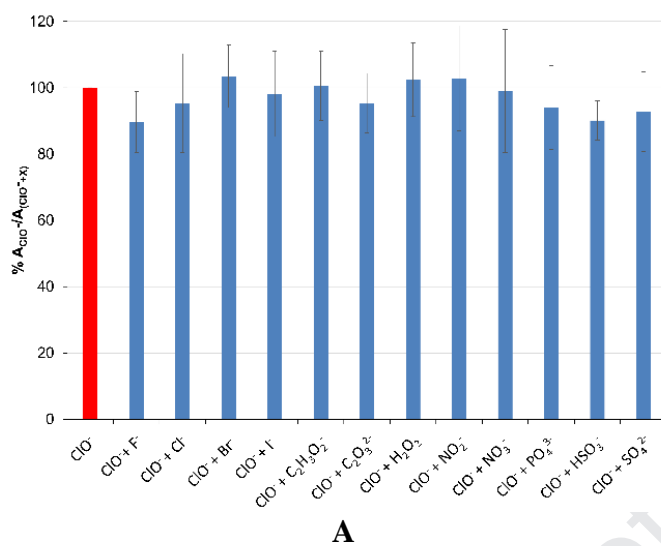
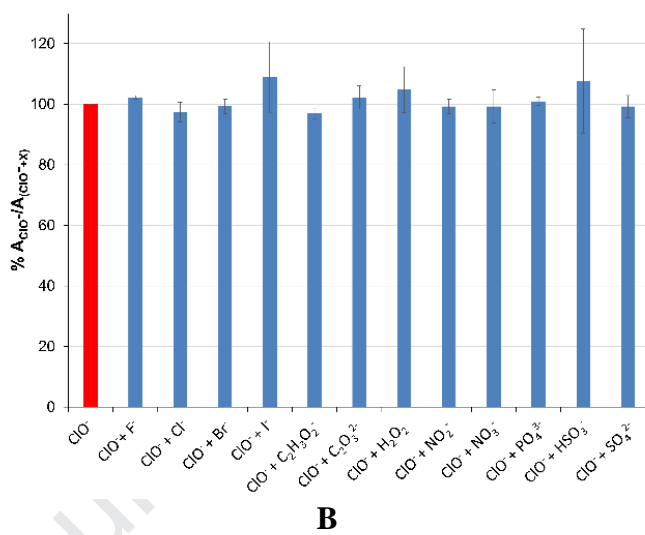


Figure 7. Absorption changes of sensor (1.0×10^{-5} M) upon the addition of various anions and H_2O_2 (5 equiv) in water/MeCN (2:1, v/v) media at pH = 7.2. A: **5a**, B: **5b** and C: **5c**.

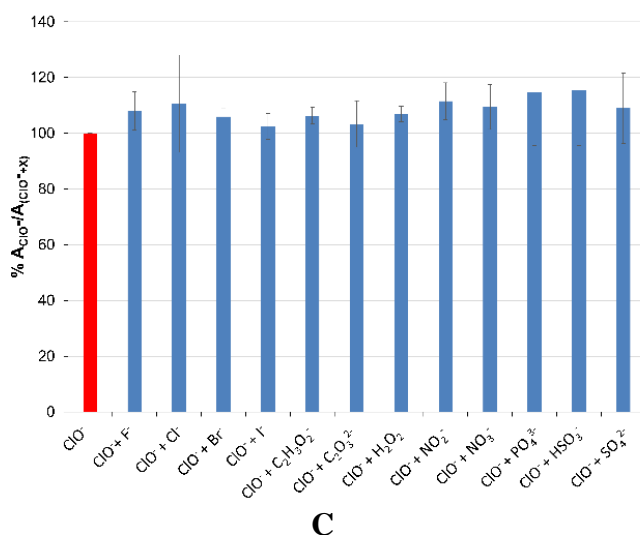
The competition experiments were conducted in the presence of ClO^- mixed with 10 equivalents of the other relevant anions, such as F^- , Cl^- , Br^- , I^- , CH_3COO^- , ClO^- , CO_3^{2-} , NO_2^- , NO_3^- , PO_4^{3-} , HSO_3^- and SO_4^{2-} . Competitive experiments performed in triplicate showed that **5b** yielded the higher recovery and lower RSD values than those of **5a** and **5c** (Figure 8). Although, sensors showed some selectivity toward H_2O_2 , experimental result indicated that H_2O_2 has had no obvious interference for the detection of ClO^- .



A



B



C

Figure 8. Effect of the competitive anions (5.0×10^{-5} M) on the interaction between sensors (1.0×10^{-5} M) in water/MeCN (2:1, v/v) media at pH = 7.2. A: **5a**, B: **5b** and C: **5c**

The linear working ranges of the sensors were obtained by successive additions of solution of hypochlorite into analysis media (Figure 9). Then calibration curves were established in order to calculate detection limit of the sensors. The experiment was performed three times, with triplicate samples in the individual experiments. A calibration curve for OCl^- concentration vs absorption was obtained for sensing experiments, and error bars given in Figure 10 represents the standard error for triplicate samples. The detection limits were calculated as 2.83×10^{-8} M, 2.10×10^{-8} M and 2.60×10^{-8} M for **5a**, **5b** and **5c**, respectively. The results are tabulated and compared with literature data in Table 3. As seen in Table 3, **5a-c** displayed highly selective and sensitive response toward OCl^- . A detailed spectrophotometric analysis for **5a** and **5c** is given in Figure S. 23 in Supplementary file.

Table 3. A comparison table about the detection limits for ClO^- .

	Working range, mol L ⁻¹	LOD, mol L ⁻¹	Reference
Cyanine	NA	1.00×10^{-7}	[31]
Quinolone	8.00×10^{-7} to 1.25×10^{-5}	8.90×10^{-8}	[32]
Chromenylium-cyanine	8.30×10^{-6} to 1.7×10^{-6}	2.10×10^{-8}	This work
Coumarine	NA	0.90×10^{-9}	[33]

NA: Not available

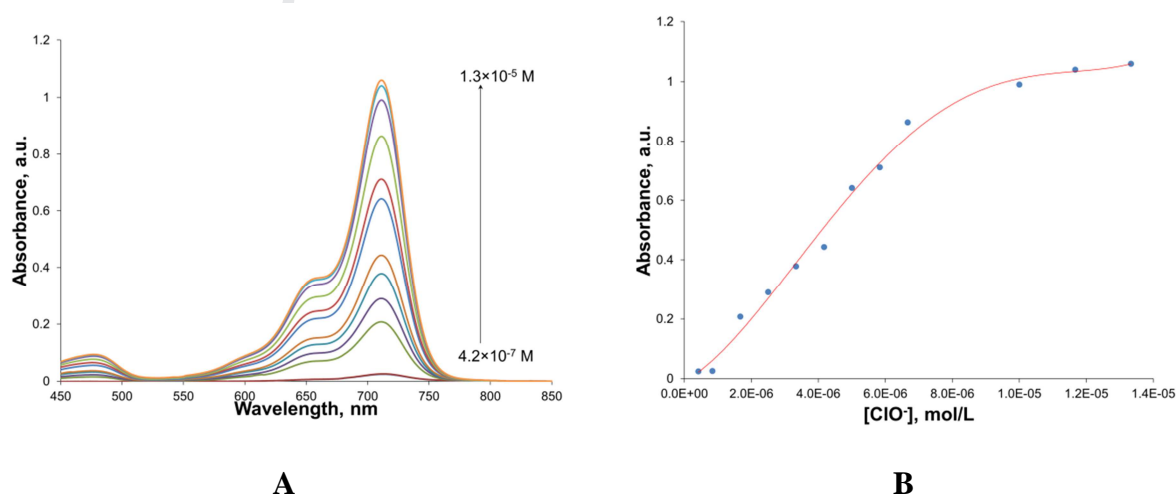


Figure 9. Optical responses of the **5b** to hypochlorite ion sensors in water/MeCN (2:1, v/v) media at pH = 7.2. A, varying in terms of molar concentration between 4.2×10^{-7} and 1.3×10^{-6} M.

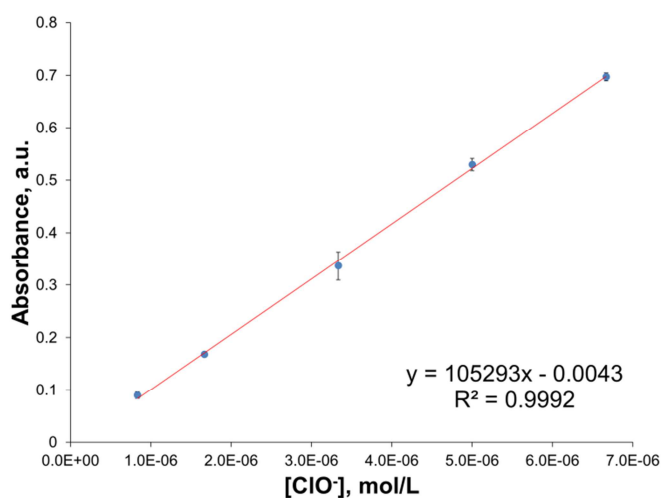


Figure 10. The calibration curve for OCl^- sensing experiments was calculated by a least-squares curve-of-best-fit procedure for **5b**.

Accuracy and precision of the sensors were tested in tap water samples. OCl^- ion was not detected in tap water, and all experiments were performed on contaminated water samples. Recovery values higher than 94% were obtained for all the sensors. As seen in Table 4, **5a** and **5c** showed lower repeatability for concentrations lower than 5.00 μM of the OCl^- . The RSD data calculated for **5b** showed that values of repeatability were acceptable for the concentration range of 1.67–6.70 μM . The higher repeatability could be related to polarization of imine double bond by electron-withdrawing hydroxyl group on aromatic ring, which would favor the complexation of Cu^{2+} ion [34].

Table 4. Results for the determination of hypochlorite in tap water samples.

Sensor	Added (μM)	Recovery (%)	RSD(n=3)
5a	1.67	100.82	5.03
	5.00	99.16	2.24
	6.70	100.41	0.97
5b	1.67	105.42	2.85
	5.00	94.60	3.81
	6.70	102.71	1.67
5c	1.67	102.74	16.87
	5.00	97.28	1.12
	6.70	101.37	3.76

3.2. Theoretical Calculations

The molecular structures of the sensors have been investigated by density functional theory (DFT) in the gas phase. Theoretical calculations have been performed using the GAMESS 2018 program [35], and data were visualized by Gabedit [36]. The Becke-3-Lee-Yang-Parr (B3LYP) exchange-correlation functional with a 6-31G(d, p) basis set for the H, C, N and O and LanL2Dz for the Cu atom were used for geometric optimizations [37,38]. No imaginary frequency was obtained in vibrational frequency calculations for optimized geometries, which demonstrated that all of the theoretical structures are at a minimum on the potential energy surface. DFT calculations showed that the sensors have almost planar geometry with a dihedral angle between the chromenylium-cyanine framework and the indole moiety close to 0° (Figure 11A). In addition, DFT calculations revealed that the spiro lactam ring was perpendicular to the

chromenylium-cyanine framework. It indicated that the theoretical results were quite compatible with the single crystal X-ray diffraction analysis.

The sensor is likely to coordinate with Cu^{2+} via phenolic O, amido N and carbonyl O atom resulting in the ring opening reaction of the spirocyclic unit, as seen Figure 11B [39]. The geometry of **5b**- Cu^{2+} complex was optimized by using different basis set and different functional combinations and computed electronic transitions for corresponding geometries were compared with the experimental results (Table S. 3). Calculations showed that SDD/B3LYP yields accurate prediction for electronic spectra. According to DFT data, the low-energy optical transitions can be assigned to $\pi \rightarrow \pi^*$ transition localized on the Schiff base unit and chromenylium rings, and shoulder at 650 nm in experimental spectrum could be assigned to ligand to metal charge transfer transition (LMCT) [40] (see Figure S. 17 for detailed analysis).

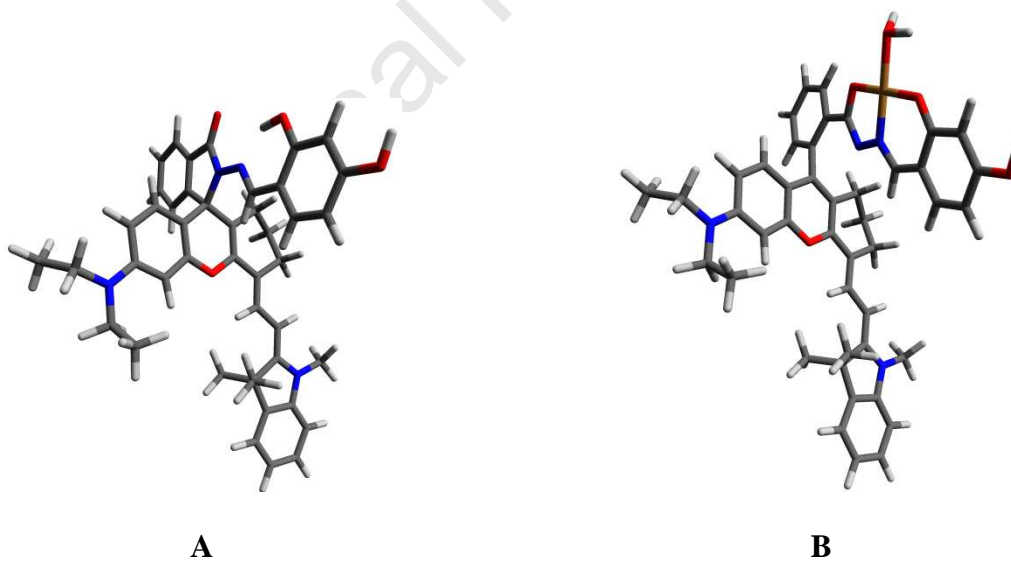


Figure 11. DFT optimized geometries of **5b** and its Cu^{2+} complex.

4. Conclusion

In summary, we developed a series of chromenylium–cyanine based Schiff base sensor to monitor OCl^- ion in aqueous media. Colorimetric response of the sensors to OCl^- ion was obtained by Cu^{2+} induced spirocyclic ring opening of the chromenylium–cyanine. An absorption enhancement was observed at near-IR region a result of complexation of the sensors with Cu^{2+} that generated by oxidation of Cu^+ ions upon the addition of OCl^- in analysis media. The results indicated that sensors exhibit excellent selectivity toward OCl^- and could be used as a selective colorimetric probe for detecting OCl^- ion in aqueous samples. The detection performances of the sensors were also tested by means of RSD% in tap water, and it was found that the sensors seem useful for the determination of the OCl^- in real samples.

Acknowledgement

This work is supported by The Scientific and Technological Research Council of Turkey (TÜBİTAK) project number 217Z250. The numerical calculations reported in this paper were fully performed at TUBITAK ULAKBİM, High Performance and Grid Computing Center (TRUBA resources).

References

- [1] Q. Xu, K.-A. Lee, S. Lee, K.M. Lee, W.-J. Lee, J. Yoon, A Highly Specific Fluorescent Probe for Hypochlorous Acid and Its Application in Imaging Microbe-Induced HOCl Production, *J. Am. Chem. Soc.* 135 (2013) 9944–9949. <https://doi.org/10.1021/ja404649m>.
- [2] D. Wu, L. Chen, Q. Xu, X. Chen, J. Yoon, Design Principles, Sensing Mechanisms, and Applications of Highly Specific Fluorescent Probes for HOCl/OCl⁻, *Acc. Chem.*

- Res. 52 (2019) 2158–2168. <https://doi.org/10.1021/acs.accounts.9b00307>.
- [3] W. Ma, Y. Ding, M. Zhang, S. Gao, Y. Li, C. Huang, G. Fu, Nature-inspired chemistry toward hierarchical superhydrophobic, antibacterial and biocompatible nanofibrous membranes for effective UV-shielding, self-cleaning and oil-water separation, *J. Hazard. Mater.* 384 (2020) 121476. <https://doi.org/10.1016/j.jhazmat.2019.121476>.
- [4] S. Goswami, S. Das, K. Aich, P.K. Nandi, K. Ghoshal, C.K. Quah, M. Bhattacharyya, H.-K. Fun, H.A. Abdel-Aziz, A rhodamine-quinoline based chemodosimeter capable of recognising endogenous OCI^- in human blood cells, *RSC Adv.* 4 (2014) 24881–24886. <https://doi.org/10.1039/c4ra03200d>.
- [5] Y.-R. Zhang, X.-P. Chen, Jing-Shao, J.-Y. Zhang, Q. Yuan, J.-Y. Miao, B.-X. Zhao, A ratiometric fluorescent probe for sensing HOCl based on a coumarin-rhodamine dyad., *Chem. Commun. (Camb).* 50 (2014) 14241–4. <https://doi.org/10.1039/c4cc05976j>.
- [6] H.J. Lee, M.J. Cho, S.K. Chang, Ratiometric Signaling of Hypochlorite by the Oxidative Cleavage of Sulfonhydrazide-Based Rhodamine-Dansyl Dyad, *Inorg. Chem.* 54 (2015) 8644–8649. <https://doi.org/10.1021/acs.inorgchem.5b01284>.
- [7] X. Lou, Y. Zhang, J. Qin, Z. Li, Colorimetric hypochlorite detection using an azobenzene acid in pure aqueous solutions and real application in tap water, *Sensors Actuators, B Chem.* 161 (2012) 229–234. <https://doi.org/10.1016/j.snb.2011.10.024>.
- [8] X. Lou, Y. Zhang, Q. Li, J. Qin, Z. Li, A highly specific rhodamine-based colorimetric probe for hypochlorites: a new sensing strategy and real application in tap water, *Chem. Commun.* 47 (2011) 3189–3191. <https://doi.org/10.1039/C0CC04911E>.
- [9] Y. Huang, M. Wang, Z. Yang, M. She, S. Wang, High efficient probes with Schiff base functional receptors for hypochlorite sensing under physiological conditions, *Chinese Chem. Lett.* 25 (2014) 1077–1081. <https://doi.org/10.1016/j.ccllet.2014.05.011>.
- [10] S. Goswami, A.K. Das, A. Manna, A.K. Maity, P. Saha, C.K. Quah, H.K. Fun, H.A.

- Abdel-Aziz, Nanomolar detection of hypochlorite by a rhodamine-based chiral hydrazide in absolute aqueous media: Application in tap water analysis with live-cell imaging, *Anal. Chem.* 86 (2014) 6315–6322. <https://doi.org/10.1021/ac500418k>.
- [11] X. Chen, X. Wang, S. Wang, W. Shi, K. Wang, H. Ma, A highly selective and sensitive fluorescence probe for the hypochlorite anion, *Chem. - A Eur. J.* 14 (2008) 4719–4724. <https://doi.org/10.1002/chem.200701677>.
- [12] Y. Long, J. Zhou, M.P. Yang, X.J. Liu, M. Zhang, B.Q. Yang, Highly selective, sensitive and naked-eye fluorescence probes for the direct detection of hypochlorite anion and their application in biological environments, *Sensors Actuators, B Chem.* 232 (2016) 327–335. <https://doi.org/10.1016/j.snb.2016.03.157>.
- [13] Y. Wei, D. Cheng, T. Ren, Y. Li, Z. Zeng, L. Yuan, Design of NIR Chromenylium-Cyanine Fluorophore Library for “switch-ON” and Ratiometric Detection of Bio-Active Species in Vivo, *Anal. Chem.* 88 (2016) 1842–1849. <https://doi.org/10.1021/acs.analchem.5b04169>.
- [14] X. Zhu, L. Yuan, X. Hu, L. Zhang, Y. Liang, S. He, X.-B. Zhang, W. Tan, Construction of a fluorine substituted chromenylium-cyanine near-infrared fluorophore for ratiometric sensing, *Sensors Actuators B Chem.* 259 (2018) 219–225. <https://doi.org/10.1016/j.snb.2017.12.008>.
- [15] R. Flores-Cruz, R. López-Arteaga, L. Ramírez-Vidal, F. López-Casillas, A. Jiménez-Sánchez, Unravelling the modus-operandi of chromenylium-cyanine fluorescent probes: a case study, *Phys. Chem. Chem. Phys.* 21 (2019) 15779–15786. <https://doi.org/10.1039/C9CP03256H>.
- [16] X. Jiao, C. Liu, S. He, L. Zhao, X. Zeng, Highly selective and sensitive ratiometric near-infrared fluorescent probe for real-time detection of Hg²⁺ and its bioapplications in live cells, *Dye. Pigment.* 160 (2019) 86–92.

- <https://doi.org/10.1016/j.dyepig.2018.07.040>.
- [17] K. Karaoglu, A new chromenylium-cyanine chemosensor for switch-ON near-infrared copper (II) sensing, *J. Mol. Struct.* (2019) 127640. <https://doi.org/10.1016/j.molstruc.2019.127640>.
- [18] M. Dong, T.H. Ma, A.J. Zhang, Y.M. Dong, Y.W. Wang, Y. Peng, A series of highly sensitive and selective fluorescent and colorimetric “off-on” chemosensors for Cu (II) based on rhodamine derivatives, *Dye. Pigment.* 87 (2010) 164–172. <https://doi.org/10.1016/j.dyepig.2010.03.015>.
- [19] L. Yuan, W. Lin, Y. Yang, H. Chen, A unique class of near-infrared functional fluorescent dyes with carboxylic-acid-modulated fluorescence ON/OFF switching: Rational design, synthesis, optical properties, theoretical calculations, and applications for fluorescence imaging in living animals, *J. Am. Chem. Soc.* 134 (2012) 1200–1211. <https://doi.org/10.1021/ja209292b>.
- [20] G.M. Sheldrick, A short history of SHELX, *Acta Crystallogr. Sect. A Found. Crystallogr.* 64 (2008) 112–122. <https://doi.org/10.1107/S0108767307043930>.
- [21] G.M. Sheldrick, Crystal structure refinement with SHELXL, *Acta Crystallogr. Sect. C Struct. Chem.* 71 (2015) 3–8. <https://doi.org/10.1107/S2053229614024218>.
- [22] O. V. Dolomanov, L.J. Bourhis, R.J. Gildea, J.A.K. Howard, H. Puschmann, OLEX2 : a complete structure solution, refinement and analysis program, *J. Appl. Crystallogr.* 42 (2009) 339–341. <https://doi.org/10.1107/S0021889808042726>.
- [23] A. Rakshit, K. Khatua, V. Shanbhag, P. Comba, A. Datta, Cu 2+ selective chelators relieve copper-induced oxidative stress in vivo, *Chem. Sci.* 9 (2018) 7916–7930. <https://doi.org/10.1039/C8SC04041A>.
- [24] G.K. Vegesna, J. Janjanam, J. Bi, F.T. Luo, J. Zhang, C. Olds, A. Tiwari, H. Liu, PH-activatable near-infrared fluorescent probes for detection of lysosomal pH inside living

- cells, *J. Mater. Chem. B.* 2 (2014) 4500–4508. <https://doi.org/10.1039/c4tb00475b>.
- [25] S. Gao, G. Tang, D. Hua, R. Xiong, J. Han, S. Jiang, Q. Zhang, C. Huang, Stimuli-responsive bio-based polymeric systems and their applications, *J. Mater. Chem. B.* 7 (2019) 709–729. <https://doi.org/10.1039/C8TB02491J>.
- [26] M. Zhang, W. Ma, J. Cui, S. Wu, J. Han, Y. Zou, C. Huang, Hydrothermal synthesized UV-resistance and transparent coating composited superoleophilic electrospun membrane for high efficiency oily wastewater treatment, *J. Hazard. Mater.* 383 (2020) 121152. <https://doi.org/10.1016/j.jhazmat.2019.121152>.
- [27] Z. Xu, L. Zhang, R. Guo, T. Xiang, C. Wu, Z. Zheng, F. Yang, A highly sensitive and selective colorimetric and off-on fluorescent chemosensor for Cu²⁺ based on rhodamine B derivative, *Sensors Actuators, B Chem.* 156 (2011) 546–552. <https://doi.org/10.1016/j.snb.2011.01.066>.
- [28] M. Li, Y. Sun, L. Dong, Q.-C. Feng, H. Xu, S.-Q. Zang, T.C.W. Mak, Colorimetric recognition of Cu²⁺ and fluorescent detection of Hg²⁺ in aqueous media by a dual chemosensor derived from rhodamine B dye with a NS2 receptor, *Sensors Actuators B Chem.* 226 (2016) 332–341. <https://doi.org/10.1016/J.SNB.2015.11.132>.
- [29] Y. Liu, Q. Su, M. Chen, Y. Dong, Y. Shi, W. Feng, Z.Y. Wu, F. Li, Near-Infrared Upconversion Chemodosimeter for In Vivo Detection of Cu²⁺ in Wilson Disease, *Adv. Mater.* (2016) 6625–6630. <https://doi.org/10.1002/adma.201601140>.
- [30] Z. Xu, H. Wang, Z. Chen, H. Jiang, Y. Ge, Near-infrared fluorescent probe for selective detection of Cu²⁺ in living cells and in Vivo, *Spectrochim. Acta - Part A Mol. Biomol. Spectrosc.* (2019). <https://doi.org/10.1016/j.saa.2019.03.062>.
- [31] X. Zhang, W. Zhao, B. Li, W. Li, C. Zhang, X. Hou, J. Jiang, Y. Dong, Ratiometric fluorescent probes for capturing endogenous hypochlorous acid in the lungs of mice, *Chem. Sci.* 9 (2018) 8207–8212. <https://doi.org/10.1039/C8SC03226B>.

- [32] Z. Mao, M. Ye, W. Hu, X. Ye, Y. Wang, H. Zhang, C. Li, Z. Liu, Design of a ratiometric two-photon probe for imaging of hypochlorous acid (HClO) in wounded tissues, *Chem. Sci.* 9 (2018) 6035–6040. <https://doi.org/10.1039/C8SC01697F>.
- [33] D. Shi, S. Chen, B. Dong, Y. Zhang, C. Sheng, T.D. James, Y. Guo, Evaluation of HOCl-generating anticancer agents by an ultrasensitive dual-mode fluorescent probe, *Chem. Sci.* 10 (2019) 3715–3722. <https://doi.org/10.1039/C9SC00180H>.
- [34] P. Maślewski, D. Wyrzykowski, M. Witwicki, A. Dołęga, Histaminol and Its Complexes with Copper(II) - Studies in Solid State and Solution, *Eur. J. Inorg. Chem.* 2018 (2018) 1399–1408. <https://doi.org/10.1002/ejic.201701411>.
- [35] M.W. Schmidt, K.K. Baldridge, J.A. Boatz, S.T. Elbert, M.S. Gordon, J.H. Jensen, S. Koseki, N. Matsunaga, K.A. Nguyen, S. Su, T.L. Windus, M. Dupuis, J.A. Montgomery, General atomic and molecular electronic structure system, *J. Comput. Chem.* 14 (1993) 1347–1363. <https://doi.org/10.1002/jcc.540141112>.
- [36] A.-R. Allouche, Gabedit-A graphical user interface for computational chemistry softwares, *J. Comput. Chem.* 32 (2011) 174–182. <https://doi.org/10.1002/jcc.21600>.
- [37] A.D. Becke, A new mixing of Hartree–Fock and local density-functional theories, *J. Chem. Phys.* 98 (1993) 1372. <https://doi.org/10.1063/1.464304>.
- [38] P.C.C. Hariharan, J.A. a. Pople, The influence of polarization functions on molecular orbital hydrogenation energies, *Theor. Chim. Acta.* 28 (1973) 213–222. <https://doi.org/10.1007/BF00533485>.
- [39] K. Wechakorn, S. Prabpai, K. Suksen, P. Kanjanasirirat, Y. Pewkliang, S. Borwornpinyo, P. Kongsaree, A rhodamine-triazole fluorescent chemodosimeter for Cu²⁺ detection and its application in bioimaging, *Luminescence.* 33 (2018) 64–70. <https://doi.org/10.1002/bio.3373>.
- [40] X.-Q. Ran, J.-K. Feng, W.-Y. Wong, A.-M. Ren, S.-Y. Poon, C.-C. Sun, Theoretical

study on photophysical properties of angular-shaped mercury(II) bis(acetylide) complexes as light-emitting materials, Chem. Phys. 368 (2010) 66–75. <https://doi.org/10.1016/j.chemphys.2009.12.019>.

Journal Pre-proof

Highlights

- A series of chromenylium-cyanine sensors were designed for ClO^- sensing.
- Spirocyclic ring-opening reaction by coordination of Cu^{2+} was observed.
- The sensors exhibited colorimetric response to hypochlorite ion at near-IR region.

Journal Pre-proof

Biographies

Kaan Karaoglu obtained his PhD degree in Recep Tayyip Erdogan University Turkey in 2014. His research interests concentrate on design of colorimetric/fluorometric chemosensor.

Kerem Kaya is a researcher at Istanbul Technical University, Chemistry Department and also operator of the single-crystal X-Ray device of the department. His research focuses are chemical crystallography and photopolymerization.

Ismail Yilmaz received his M.S. and Ph.D. degrees in Chemistry from Istanbul Technical University, Turkey in 1992 and 1996. He spent one year on research of electrochemistry and spectroelectrochemistry of phthalocyanines as a visiting scientist and postdoctoral fellow in Professor Kadish's group in the University of Houston. He is currently working as a professor at the Department of Chemistry of Istanbul Technical University. His research interests include the design and construction of multi-channel ion-selective chemosensors.

Declaration of interests

The authors declare that they have no known competing financial interests or personal relationships that could have appeared to influence the work reported in this paper.

The authors declare the following financial interests/personal relationships which may be considered as potential competing interests:

Journal Pre-proof